Prandtl number scaling of natural convection of the flow on a heated inclined flat plate

Suvash C. Saha[1] Y. T. Gu[2]

(Received 8 January 2012; revised 7 July 2012)

Abstract

A new scaling analysis has been performed for the unsteady natural convection boundary layer under a downward facing inclined plate with uniform heat flux. The development of the thermal or viscous boundary layers is classified into three distinct stages including an early stage, a transitional stage and a steady stage, which is clearly identified in the analytical as well as in numerical results. Earlier scaling shows that the existing scaling laws of the boundary layer thickness, velocity and steady state time scales for the natural convection flow on a heated plate of uniform heat flux provide a very poor prediction of the Prandtl number dependency. However, those scalings performed very well with Rayleigh number and aspect ratio dependency. In this study, a modified Prandtl number scaling is developed using a triple-layer integral approach for Prandtl number larger than unity.

http://journal.austms.org.au/ojs/index.php/ANZIAMJ/article/view/5089 gives this article, © Austral. Mathematical Soc. 2012. Published July 16, 2012. ISSN 1446-8735. (Print two pages per sheet of paper.)

In comparison to the direct numerical simulations, the new scaling performs considerably better than the previous scaling.

Contents

1 Introduction

Natural convection heat transfer along an inclined surface is frequently encountered in nature and in engineering devices, such as solar water heaters and attic roof spaces. Parallel to the classic cases, such as vertical or horizontal plates, studies on natural convection along an inclined plate have also received considerable attention of the researchers due to its direct engineering application [1, 2, 3, 4, 5, 6]. Several methodologies are being used including experimental, numerical and mathematical analysis previously. Recently, scaling analysis was widely used to analyse the transient boundary layer de-

velopment adjacent to the downward facing inclined surface for both heating and cooling cases [3, 4, 5, 6].

After orientation of scaling analysis for both unsteady and steady boundary layer in a rectangular enclosure by Patterson and Imberger [7], scaling analysis is extensively used in many other geometries and thermal forcing conditions [8, 9, 10, 11, 12, 13, 14]. The main reason for considering scaling analysis is that it is a cost-effective way that is applied for understanding the physical mechanism of the fluid flow and heat transfer before performing any laborious work. We know not all terms of the governing equations are important at all the time of boundary layer development. Therefore, the scaling analysis is performed by comparing relative terms (two or three dominant terms) in the governing equation in a specific stage of the flow development. However, the obtained results are correct to one order of magnitude.

Only sudden and ramp temperature boundary conditions are considered to perform the scaling analysis of the semi-infinite inclined flat plate. However, scaling analysis of the boundary layer due to uniform heat flux on the boundary is still unrevealed for this geometry. Therefore, we attempt to deal with the scaling analysis as a result of uniform heat flux condition on the inclined surface in this study. To perform this, a recently introduced three-region scaling analysis for the development of the boundary layer adjacent to a downward facing inclined heated flat plate is considered [3, 4, 10]. Emphasis has been given to show the dependency of Prandtl number ($Pr > 1$). We have achieved the scaling relations of the velocity, thermal and viscous layer thicknesses in the different stages of the boundary layer development. We have also obtained the time scale of the transition of the flow to a steady state. The scaling results are verified by a series of numerical simulations for different flow parameters: Rayleigh number (Ra), Prandtl number (Pr) and slope of the plate (A). The numerical results agree very well with the scaling results.

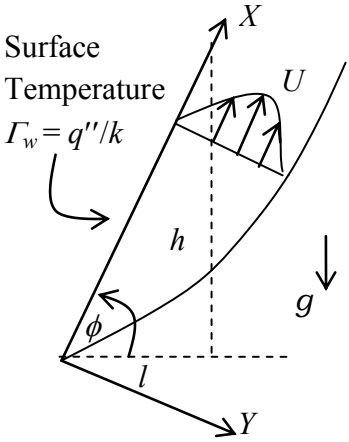

Figure 1: Schematic of the geometry and the coordinate system.

2 Formulation and scaling analysis

We consider the flow resulting from an initially motionless and isothermal Newtonian fluid with $Pr > 1$ adjacent to a downward facing inclined heated plate due to uniform heat flux. As seen in Figure 1, an inclined flat plate of heated length L is placed in the fluid which is initially stationary at a temperature T_0. Considering the plate as the hypotenuse of a right angled triangle, then the height is h, the length of the base is l and the angle that the plate makes with the base is ϕ.

The fluid flow and heat transfer under the inclined plate is governed by the following two dimensional Navier–Stokes and energy equations with the Boussinesq approximation:

$$\frac{\partial U}{\partial X} + \frac{\partial V}{\partial Y} = 0\,, \tag{1}$$

$$\frac{\partial U}{\partial t} + U\frac{\partial U}{\partial X} + V\frac{\partial U}{\partial Y} = -\frac{1}{\rho}\frac{\partial P}{\partial X} + \nu\left(\frac{\partial^2 U}{\partial X^2} + \frac{\partial^2 U}{\partial Y^2}\right) + g\beta\sin\phi T\,, \tag{2}$$

$$\frac{\partial V}{\partial t} + U\frac{\partial V}{\partial X} + V\frac{\partial V}{\partial Y} = -\frac{1}{\rho}\frac{\partial P}{\partial Y} + \nu\left(\frac{\partial^2 V}{\partial X^2} + \frac{\partial^2 V}{\partial Y^2}\right) + g\beta\cos\phi T\,, \tag{3}$$

$$\frac{\partial T}{\partial t} + U\frac{\partial T}{\partial X} + V\frac{\partial T}{\partial Y} = \kappa\left(\frac{\partial^2 T}{\partial X^2} + \frac{\partial^2 T}{\partial Y^2}\right). \tag{4}$$

Initially, the fluid is quiescent and isothermal. The temperature condition on the plate is

$$\frac{\partial T}{\partial \mathbf{n}} = -\Gamma_w = -\frac{q''}{k}, \tag{5}$$

where $\mathbf{n}$ is the unit vector normal to the plate surface.

We know that the flow development due to natural convection is determined by three governing parameters: the Rayleigh number (Ra), the Prandtl number (Pr) and the slope (A). They are defined, respectively, as

$$\mathrm{Ra} = \frac{g\beta\Gamma_w h^4}{\kappa\nu}\,, \quad \mathrm{Pr} = \frac{\nu}{\kappa}\,, \quad A = \frac{h}{l}\,. \tag{6}$$

2.1 Early stage

Figure 2 shows a three-region structure for the boundary layers for $\mathrm{Pr} > 1$. As seen, the peak velocity U_m occurs within the thermal boundary layer, δ_T, at a distance $\delta_T - \delta_i$ (viscous inner layer) from the wall. Also, there is a region of flow outside δ_T where the flow is not directly driven by the buoyancy, but is the result of diffusion of momentum. Therefore, in regions I and II, the balance is between viscosity and buoyancy. However, in region III the balance is between viscosity and inertia, since there is no buoyancy there. A brief of the derivation of scalings is presented here due to brevity. The detailed derivation is to be found in the work of Saha et al. [3, 4, 10, 13]. Initially, the balancing terms in the energy equation (4) is the unsteady term and the conduction term, which gives

$$\delta_T \sim \kappa^{1/2} t^{1/2}, \tag{7}$$

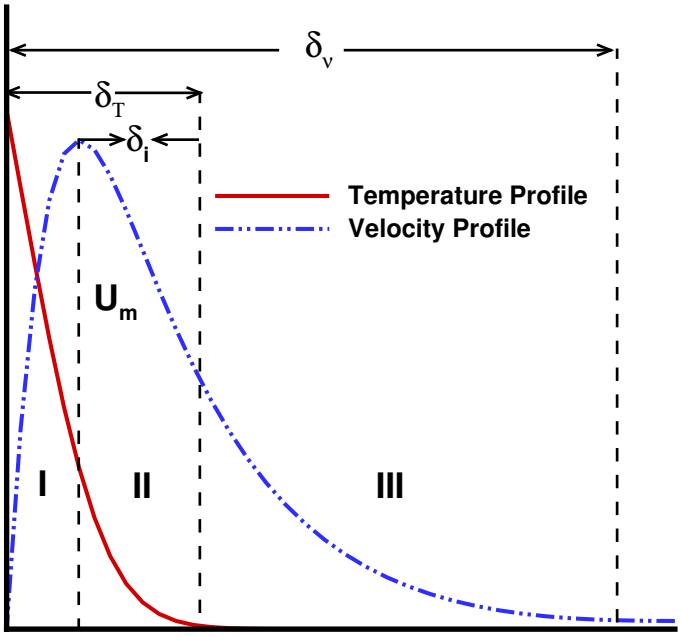

Figure 2: A schematic of the temperature and velocity profiles normal to the inclined plate at its mid point: the thermal boundary layer is $O(\delta_T)$; the viscous boundary layer is $O(\delta_v)$; and δ_i is the scale for the distance between the maximum velocity and δ_T. Regions I, II and III are shown on the figure.

This scaling is valid until the convection term becomes important. At the same time, the correct balance in the momentum equation (2) is between the viscosity and the buoyancy,

$$0 \sim \nu \frac{\partial^2 U}{\partial Y^2} + g\beta\Delta T \sin\phi \tag{8}$$

where ΔT, the total temperature variation over the boundary layer, is of $O(\Gamma_w \delta_T)$. Using (7), this is written as

$$\Delta T \sim \Gamma_w \kappa^{1/2} t^{1/2}. \tag{9}$$

In region I (the inner viscous layer), the balance (8) gives

$$U_m \sim \frac{g\beta\Gamma_w\delta_T \sin\phi}{\nu}(\delta_T - \delta_i)^2 \tag{10}$$

By integrating (8) from $(\delta_T - \delta_i)$ to δ_T we get the velocity scale in region II,

$$U_m \sim \frac{g\beta\Gamma_w\delta_T \sin\phi}{\nu}\delta_i(\delta_\nu - \delta_T + \delta_i)^2. \tag{11}$$

From (10) and (11) we obtain

$$\delta_i \sim \frac{\delta_T^2}{\delta_T + \delta_\nu} \tag{12}$$

where $\delta_\nu \sim \nu^{1/2}t^{1/2}$. Consequently,

$$\delta_T - \delta_i \sim \delta_T - \frac{\delta_T}{1 + Pr^{1/2}} \sim \frac{Pr^{1/2}}{1 + Pr^{1/2}}\delta_T\,, \tag{13}$$

Finally, the unsteady velocity scale becomes

$$U_m \sim \frac{Ra\,\kappa^{5/2}}{h^4}\frac{A}{(1 + A^2)^{1/2}}\left(\frac{Pr^{1/2}}{1 + Pr^{1/2}}\right)^2 t^{3/2}. \tag{14}$$

2.2 Steady stage

As time increases, more heat is convected away through the boundary layer. Hence, the boundary layer approaches a steady state when convection balances conduction, that is

$$U_m\frac{\Delta T}{L} \sim \kappa\frac{\Delta_T}{\delta_T^2}\,, \tag{15}$$

Therefore, the steady state time scale and the corresponding velocity, thermal layer thickness and surface temperature scales are obtained as

$$t_s \sim \frac{h^2}{Ra^{2/5}\,\kappa}\left(\frac{1+A^2}{A^2}\right)^{2/5}\left(\frac{1+Pr^{1/2}}{Pr^{1/2}}\right)^{4/5}, \tag{16}$$

$$U_{ms} \sim \frac{Ra^{2/5}\,\kappa}{h}\left(\frac{1+A^2}{A^2}\right)^{1/10}\left(\frac{Pr^{1/2}}{1+Pr^{1/2}}\right)^{4/5}, \tag{17}$$

$$\delta_{Ts} \sim \frac{h}{Ra^{1/5}}\left(\frac{1+A^2}{A^2}\right)^{1/5}\left(\frac{1+Pr^{1/2}}{Pr^{1/2}}\right)^{2/5}, \tag{18}$$

$$\delta_T - \delta_i \sim \frac{h}{Ra^{1/5}}\left(\frac{1+A^2}{A^2}\right)^{1/5}\left(\frac{Pr^{1/2}}{1+Pr^{1/2}}\right)^{3/5}, \tag{19}$$

$$T_{ws} \sim \Gamma_w \delta_{Ts} \sim \Gamma_w \frac{h}{Ra^{1/5}}\left(\frac{1+A^2}{A^2}\right)^{1/5}\left(\frac{1+Pr^{1/2}}{Pr^{1/2}}\right)^{2/5}. \tag{20}$$

3 Non-dimensionalization

To verify the various scales, numerical solutions of the full Navier–Stokes equations and energy were obtained for a range of Ra, Pr and A values. For convenience the following sets of expressions are used to normalize equations (1)–(4),

$$x = \frac{X}{h}, \quad y = \frac{Y}{h}, \quad u = \frac{U}{U_0}, \quad v = \frac{V}{U_0},$$
$$\tau = \frac{t}{h/U_0}, \quad p = \frac{P}{\rho U_0^2}, \quad \theta = \frac{T}{\Gamma_w h}, \tag{21}$$

where x, y, u, v, θ, p and τ are the normalized forms of X, Y, U, V, T, P and t, respectively, and where $U_0 = (\kappa\,Ra^{1/2})/h$ is the characteristic velocity scale used by Saha et al. [4].

Using the above transformations (21), the non-dimensional governing equations take the form

$$\frac{\partial u}{\partial x}+\frac{\partial v}{\partial y}=0\,, \tag{22}$$

$$\frac{\partial u}{\partial \tau}+u\frac{\partial u}{\partial x}+v\frac{\partial u}{\partial y}=-\frac{\partial p}{\partial x}+\frac{Pr}{Ra^{1/2}}\left(\frac{\partial^2 u}{\partial x^2}+\frac{\partial^2 u}{\partial y^2}\right)+Pr\,\theta\sin\phi\,, \tag{23}$$

$$\frac{\partial v}{\partial \tau}+u\frac{\partial v}{\partial x}+v\frac{\partial v}{\partial y}=-\frac{\partial p}{\partial y}+\frac{Pr}{Ra^{1/2}}\left(\frac{\partial^2 v}{\partial x^2}+\frac{\partial^2 v}{\partial y^2}\right)+Pr\,\theta\cos\phi\,, \tag{24}$$

$$\frac{\partial \theta}{\partial \tau}+u\frac{\partial \theta}{\partial x}+v\frac{\partial \theta}{\partial y}=\frac{1}{Ra^{1/2}}\left(\frac{\partial^2 \theta}{\partial x^2}+\frac{\partial^2 \theta}{\partial y^2}\right). \tag{25}$$

In the initial stage the non-dimensional scales are

$$\Delta_T\sim\theta_w\sim\frac{\tau^{1/2}}{Ra^{1/4}}\,, \tag{26}$$

$$\Delta_T-\Delta_i\sim\frac{Pr^{1/2}}{1+Pr^{1/2}}\frac{\tau^{1/2}}{Ra^{1/4}}\,, \tag{27}$$

$$u_m\sim\frac{1}{Ra^{1/4}}\frac{A}{(1+A^2)^{1/2}}\left(\frac{Pr^{1/2}}{1+Pr^{1/2}}\right)^2\tau^{3/2}. \tag{28}$$

In the steady stage the non-dimensional scales are

$$\tau_s\sim Ra^{1/10}\left(\frac{1+A^2}{A^2}\right)^{2/5}\left(\frac{1+Pr^{1/2}}{Pr^{1/2}}\right)^{4/5}, \tag{29}$$

$$u_{ms}\sim\frac{1}{Ra^{1/10}}\left(\frac{1+A^2}{A^2}\right)^{1/10}\left(\frac{Pr^{1/2}}{1+Pr^{1/2}}\right)^{4/5}, \tag{30}$$

$$\Delta_{Ts}\sim\frac{1}{Ra^{1/5}}\left(\frac{1+A^2}{A^2}\right)^{1/5}\left(\frac{1+Pr^{1/2}}{Pr^{1/2}}\right)^{2/5}, \tag{31}$$

$$\Delta_{Ts} - \Delta_{is} \sim \frac{1}{Ra^{1/5}} \left(\frac{1+A^2}{A^2}\right)^{1/5} \left(\frac{Pr^{1/2}}{1+Pr^{1/2}}\right)^{3/5}, \tag{32}$$

$$\Delta_{vs} \sim \frac{1}{Ra^{1/5}} \left(\frac{1+A^2}{A^2}\right)^{1/5} Pr^{1/2} \left(\frac{1+Pr^{1/2}}{Pr^{1/2}}\right)^{2/5}, \tag{33}$$

$$\theta_{ws} \sim \frac{1}{Ra^{1/5}} \left(\frac{1+A^2}{A^2}\right)^{1/5} \left(\frac{1+Pr^{1/2}}{Pr^{1/2}}\right)^{2/5}. \tag{34}$$

4 Numerical technique

Equations (22)–(25) were solved along with the initial and boundary conditions using the SIMPLE scheme. The Finite Volume scheme was chosen to discretize the governing equations, with the QUICK scheme approximating the advection term. The diffusion terms were discretized using central differencing with second order accurate. A second order implicit time-marching scheme was also used for the unsteady term. The detailed numerical procedure is found in the work of Saha et al. [3, 4, 5, 6]. The same geometry and mesh size considered by Saha and Khan [3] and Saha [4] were also adopted in this study.

5 Results and discussion

In this section the computed time series data of the maximum velocity parallel to the plate (u_m) are recorded along the line $x = 0.5$, which is sufficiently far from the leading edge to avoid any leading edge effect. This data validates the velocity scale.

The time series of the non-dimensional maximum velocity parallel to the plate with unsteady velocity scale (28) is plotted in Figure 3 for different values of Ra, Pr and A. Initially, all lines for the different Rayleigh numbers,

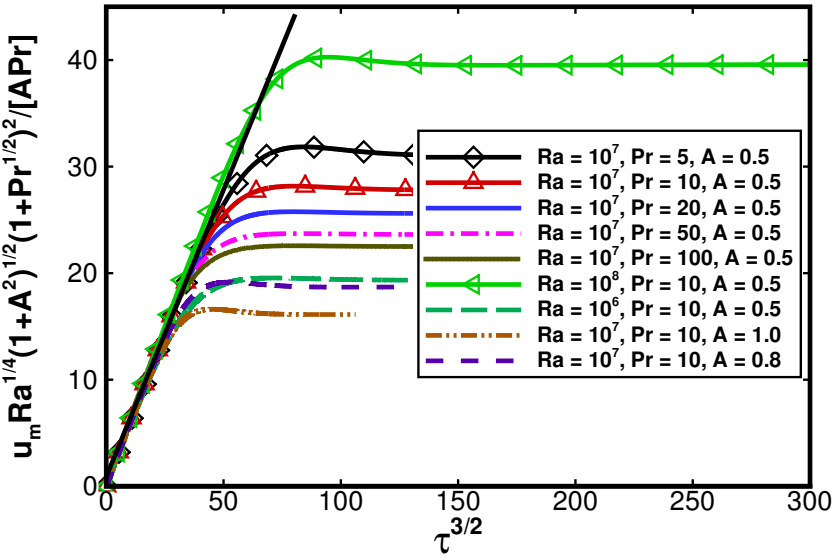

Figure 3: Time series of the maximum velocity parallel to the plate at $x = 0.5$ for all cases considered: $u_m\, Ra^{1/4}(1+A^2)^{1/2}(1+Pr^{1/2})^2/[A\, Pr]$ plotted against $\tau^{3/2}$.

Prandtl numbers and aspect ratios lie together on a straight line through the origin. This indicates that the scaling relation (28) for the unsteady velocity is appropriate.

To validate the steady state velocity scale, the time series of maximum velocity parallel to the plate is again plotted in Figure 4. Figure 4(a) represents the time series of u_m for varying three governing parameters, Ra, Pr and A. The three stages of flow development are seen clearly in this figure. In the initial stage the maximum velocity increases due to heat conduction through the heated plate. A small transition of the boundary layer, as a form of overshoot, is also seen when the conduction term in the energy equation (4) balances with the convection term. The flow becomes steady state afterwards. Figure 4(b) depicts the same time series as in Figure 4(a) but u_m and τ are scaled by u_{ms} (30) and τ_s (29) respectively. All scaled time series approach the

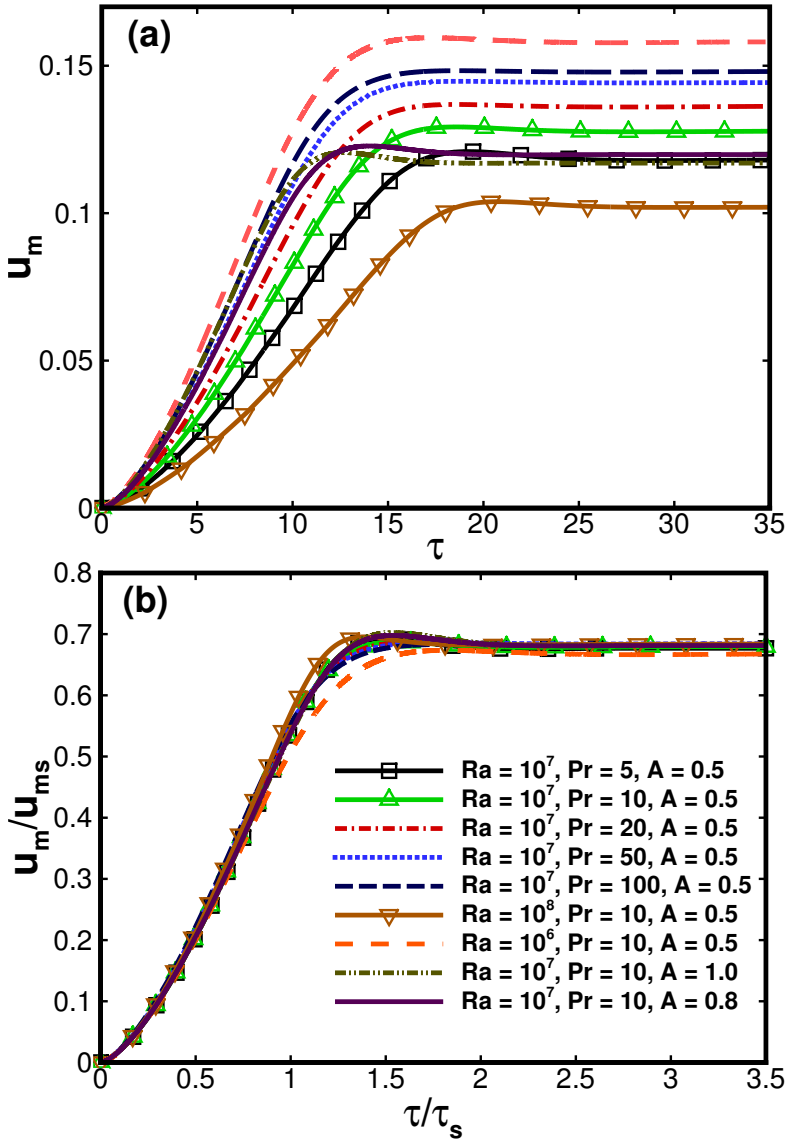

Figure 4: Time series of the maximum velocity parallel to the plate at $x = 0.5$ for all cases considered: (a) computed data and (b) $u\,Ra^{1/10}\,A^{1/5}(1+Pr^{1/2})^{4/5}/[(1+A^2)^{1/10}\,Pr^{2/5}]$ plotted against $\tau A^{4/5}\,Pr^{2/5}\,/[Ra^{1/10}(1+A^2)^{2/5}(1+Pr^{1/2})^{4/5}]$.

same horizontal straight line at the steady stage, confirming that the scaling relation (30) is the correct scaling for u_m at the steady state. Figure 4(b) also shows that the peaks of all nine scaled time series occur almost at the same scaled time, validating the scaling relation (29).

Figure 5 illustrates the numerical results of the average surface temperature of the heated inclined plate. The computed time series of the surface temperature are plotted in Figure 5(a) for different parameters considered here. There are significant effects of those parameters on the surface temperature. The temperature is normalized with its steady state scaling value (34) and the time is normalized with the steady state time scale (29) and are re-plotted in Figure 5(b). Consequently, all curves for the different parameters collapse together onto a single curve, confirming the scaling relation of temperature at the steady stage (34) and the steady state time scale (29). Thickness scale for both thermal and viscous boundary layer can be easily validated by calculating those profiles along the line $x = 0.5$ at any time of the flow development [3, 4, 10, 13, e.g.].

6 Conclusions

Unsteady fluid flow and heat transfer due to natural convection under a downward facing heated inclined flat plate is examined by scaling analysis for Prandtl number, $Pr > 1$. The scaling shows a strong Pr dependency on the velocity field in both the initial stage or the conductive phase and in the steady state stage or the convective phase. The scaling relations were verified by full numerical solutions for various parameters considered here. Numerical results demonstrate that the scaling relations are able to accurately characterize the physical behaviour in each stage of the flow development, including the initial stage, the transitional stage and the steady state stage over the Prandtl number range considered. The scaling relations are formed based on the established characteristic flow parameters of the maximum velocity in the boundary layer (u_m), the time for the boundary layer to reach

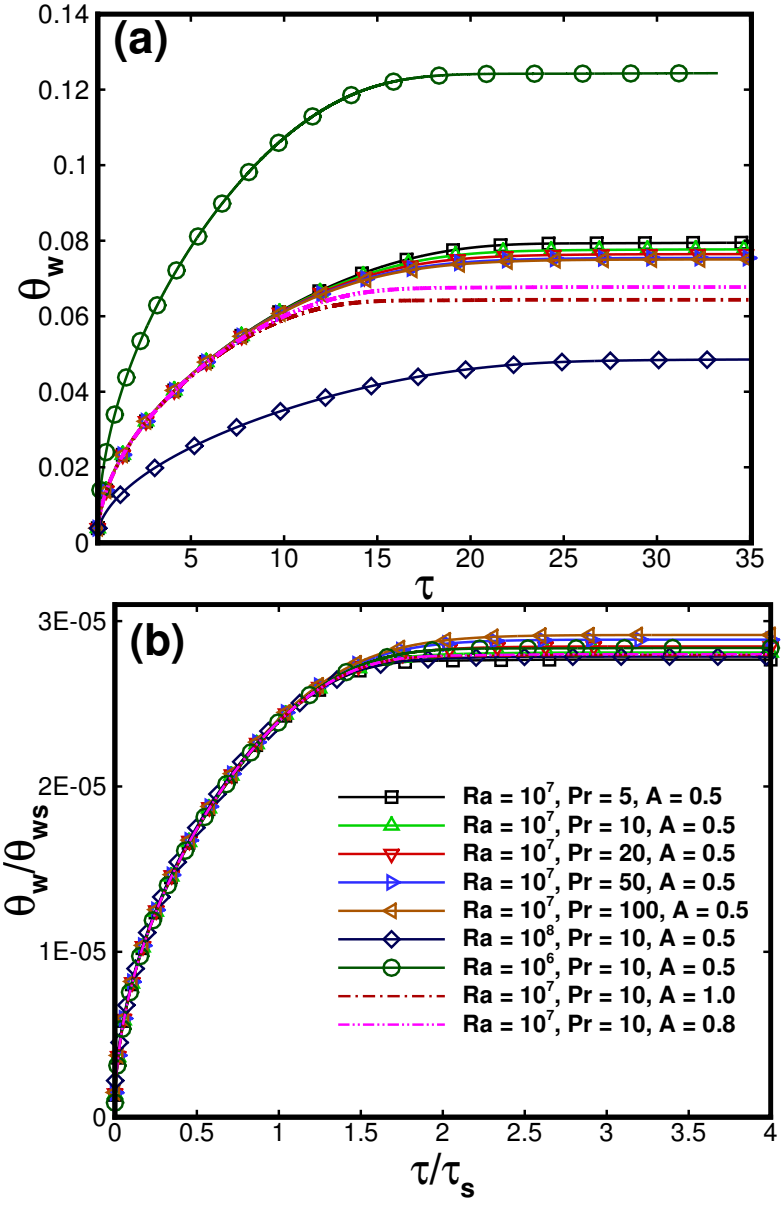

Figure 5: Time series of the surface temperature on the inclined plate for all cases considered: (a) computed data and (b) $\theta\,\mathrm{Ra}^{1/5}\,\mathrm{A}^{2/5}\,\mathrm{Pr}^{1/5}\,/[(1{+}\mathrm{A}^2)^{1/5}(1{+}\mathrm{Pr}^{1/2})^{2/5}]$ plotted against $\tau\mathrm{A}^{4/5}\,\mathrm{Pr}^{2/5}\,/[\mathrm{Ra}^{1/10}(1+\mathrm{A}^2)^{2/5}(1+\mathrm{Pr}^{1/2})^{4/5}]$.

the steady state (τ_s) and the thermal ($\Delta_T s$) and viscous ($\Delta_\nu s$) boundary layer thickness. Through comparisons of the scaling relations with the numerical simulations, we found that the scaling results agreed very well with the numerical simulations. In particular, in this study the multiple region scaling accurately predicted the Prandtl number dependency of the inner velocity length scale, $\Delta_{Ts} - \Delta_{is}$, and the velocity maximum u_m, quantities that were poorly predicted using a single region scaling.

References

[1] E. M. Sparrow, R. B. Husar, Longitudinal vortices in natural convection flow on inclined plates. *J. Fluid. Mech.* **37** (1969) 251–255. doi:10.1017/S0022112069000528 C388

[2] A. Bejan, *Convection Heat Transfer*, third ed., (2004) John Wiley and Sons. C388

[3] S. C. Saha, M. M. K. Khan, An improved boundary layer scaling with ramp heating on a sloping plate *Int. J. Heat Mass Transfer*, **55** (2012) pp. 2268–2284. doi:10.1016/j.ijheatmasstransfer.2012.01.038 C388, C389, C391, C396, C399

[4] S. C. Saha, F. Xu, M. M. Molla, Scaling analysis of the unsteady natural convection boundary layer adjacent to an inclined plate for $Pr > 1$ following instantaneous heating. *J. Heat Transfer - Transaction of ASME* **133** (2011) 112501. doi:10.1115/1.4004336 C388, C389, C391, C394, C396, C399

[5] S. C. Saha, J. C. Patterson, C. Lei, Scaling of natural convection of an inclined flat plate: Sudden cooling condition. *J. Heat Transfer - Transaction of ASME* **133** (2011) 041503. doi:10.1115/1.4002982 C388, C389, C396

[6] S. C. Saha, J. C. Patterson, C. Lei, Natural convection boundary layer adjacent to an inclined flat plate subject to sudden and ramp heating. *Int. J. Therm. Sci.* **49** (2010) 1600–1612. doi:10.1016/j.ijthermalsci.2010.03.017 C388, C389, C396

[7] J. C. Patterson, J. Imberger, Unsteady natural convection in a rectangular cavity. *J. Fluid Mech.* **100** (1980) 65–86. doi:10.1017/S0022112080001012 C389

[8] W. Lin, S. W. Armfield, Direct simulation of natural convection cooling in a vertical circular cylinder. *Int. J. Heat Mass Transfer* **42** (1999) 4117–4130. doi:10.1016/S0017-9310(99)00074-5 C389

[9] W. Lin, S. W. Armfield, J. C. Patterson, C. Lei, Prandtl number scaling of unsteady natural convection boundary layers of $\mathsf{Pr} > 1$ fluids under isothermal heating. *Phys. Rev. E* **79**, (2009) 066313. doi:10.1103/PhysRevE.79.066313 C389

[10] S. C. Saha, Unsteady natural convection in a triangular enclosure under isothermal heating. *Energy Buildings* **43** (2011) 695–703. doi:10.1016/j.enbuild.2010.11.014 C389, C391, C399

[11] S. C. Saha, J. C. Patterson, C. Lei, Natural convection in attic-shaped spaces subject to sudden and ramp heating boundary conditions. *Heat Mass Transfer* **46** (2010) 621–638. doi:10.1007/s00231-010-0607-5 C389

[12] S. C. Saha, J. C. Patterson, C. Lei, Natural convection in attics subject to instantaneous and ramp cooling boundary conditions. *Energy Buildings* **42** (2010) 1192–1204. doi:10.1016/j.enbuild.2010.02.010 C389

[13] S. C. Saha, Scaling of free convection heat transfer in a triangular cavity for $\mathsf{Pr} > 1$. *Energy Buildings* **43** (2011) 2908–2917. doi:10.1016/j.enbuild.2011.07.016 C389, C391, C399

[14] T. P. Bednarz, W. Lin, S. C. Saha, Scaling of thermo-magnetic convection. In *Proceedings of the 13th Asian Congress of Fluid Mechanics*, Dhaka, Bangladesh, (2010) 798–801. C389

Author addresses

1. **Suvash C. Saha**, School of Chemistry, Physics and Mechanical Engineering, Queensland University of Technology, Brisbane Queensland 4001, Australia.
mailto:suvash.saha@qut.edu.au

2. **Y. T. Gu**, School of Chemistry, Physics and Mechanical Engineering, Queensland University of Technology, Brisbane Queensland 4001, Australia.
mailto:yuantong.gu@qut.edu.au